Hierarchical random additive process and logarithmic scaling of generalized high order, two-point correlations in turbulent boundary layer flow

X. I. A. Yang,[1] I. Marusic,[2] and C. Meneveau[1]

[1]*Department of Mechanical Engineering and Center for Environmental and Applied Fluid Mechanics,*
The Johns Hopkins University, 3400 North Charles Street, Baltimore, Maryland 21218, USA
[2]*Department of Mechanical Engineering, University of Melbourne, Melbourne, Victoria 3010, Australia*
(Received 28 January 2016; published 13 June 2016)

Townsend [Townsend, *The Structure of Turbulent Shear Flow* (Cambridge University Press, Cambridge, UK, 1976)] hypothesized that the logarithmic region in high-Reynolds-number wall-bounded flows consists of space-filling, self-similar attached eddies. Invoking this hypothesis, we express streamwise velocity fluctuations in the inertial layer in high-Reynolds-number wall-bounded flows as a hierarchical random additive process (HRAP): $u_z^+ = \sum_{i=1}^{N_z} a_i$. Here u is the streamwise velocity fluctuation, $+$ indicates normalization in wall units, z is the wall normal distance, and a_i's are independently, identically distributed random additives, each of which is associated with an attached eddy in the wall-attached hierarchy. The number of random additives is $N_z \sim \ln(\delta/z)$ where δ is the boundary layer thickness and ln is natural log. Due to its simplified structure, such a process leads to predictions of the scaling behaviors for various turbulence statistics in the logarithmic layer. Besides reproducing known logarithmic scaling of moments, structure functions, and correlation function $\langle u_z(x)u_z(x+r)\rangle$, new logarithmic laws in two-point statistics such as $\left[\frac{3}{2}\langle u_z^2(x)u_z^2(x+r)\rangle - \frac{1}{2}\langle u_z^4(x)\rangle\right]^{1/2}$, $\left[\frac{5}{2}\langle u_z^3(x)u_z^3(x+r)\rangle - \frac{3}{2}\langle u_z(x)u_z^5(x+r)\rangle\right]^{1/3}$, etc. can be derived using the HRAP formalism. Supporting empirical evidence for the logarithmic scaling in such statistics is found from the Melbourne High Reynolds Number Boundary Layer Wind Tunnel measurements. We also show that, at high Reynolds numbers, the above mentioned new logarithmic laws can be derived by assuming the arrival of an attached eddy at a generic point in the flow field to be a Poisson process [Woodcock and Marusic, Phys. Fluids **27**, 015104 (2015)]. Taken together, the results provide new evidence supporting the essential ingredients of the attached eddy hypothesis to describe streamwise velocity fluctuations of large, momentum transporting eddies in wall-bounded turbulence, while observed deviations suggest the need for further extensions of the model.

I. INTRODUCTION

High-Reynolds-number wall-bounded flows are commonly encountered in many engineering, environmental, and geophysical flows. A robust feature of such flows is the presence of the logarithmic region, a region where neither the viscosity nor the bulk flow appears to be dynamically dominant [1–3]. One particularly effective conceptual model of wall turbulence dates back to Townsend [4], who hypothesized that the logarithmic region consists of space-filling, self-similar eddies, as shown schematically in Fig. 1(a), whose sizes scale with their distance from the wall. This attached eddy hypothesis has proven to be quite useful in providing (nontrivial) estimates on the scalings in various turbulence quantities, including turbulence intensity, Reynolds stress, single-point moments, two-point statistics, pressure fluctuations, etc., in wall-bounded flows at high Reynolds number [4–11]. The hypothesis has also guided studies of flow structures [12,13], including near-wall hairpins [14–18] and coherent vortex packets or clusters [19–25], and has provided insights into modeling of flow spectra [26–28].

Therefore it is not surprising that many efforts have been devoted to various formal mathematical formulations of the Townsend attached eddy hypothesis [4,5,10,29,30]. While details might vary among the various formalisms, all attached eddy models are based on an eddy population density
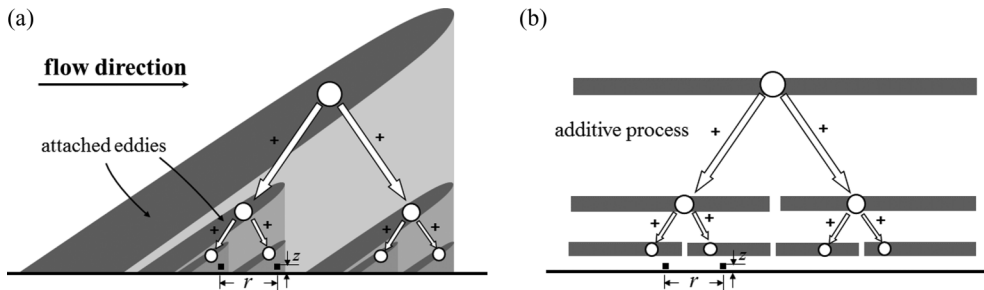
FIG. 1. (a) Sketch of the hypothesized structure of attached eddies in wall-bounded flows. The eddy population density is inversely proportional to the wall distance. On a two-dimensional plane cut as shown here, on average, the number of visible eddies doubles as the size halves. (b) A more explicit representation of the additive process.

that is inversely proportional to the wall distance, i.e., $P(z) \sim 1/z$, which is a direct consequence of the space-filling property of the hierarchical attached eddies [10].

A particularly simple version of the attached eddy hypothesis was invoked in Ref. [9] to make predictions of logarithmic scaling in single-point high-order moments. Discretizing the wall normal distance logarithmically and counting the number of attached eddies that affect a generic point at height z, namely, adding the contributions from the eddies at all heights above z up to the largest at the top of the boundary layer (at $z \sim \delta$), one obtains

$$N_z \sim \int_z^\delta P(z)\,dz \sim \ln(\delta/z). \tag{1}$$

The velocity at a point at height z is assumed to be an additive superposition of the velocity induced by each attached eddy that overlaps the particular point of interest. Taking into consideration the self-similar property of the assumed attached eddies and assuming that they are noninteracting, the instantaneous velocity at this generic point is simply modeled as a sum of identically, independently distributed (i.i.d.) random additives a_i with $\langle a_i \rangle = 0$. Denoting the instantaneous streamwise velocity normalized by friction velocity (or velocity fluctuation if its time mean is subtracted) at height z as u_z^+, a simplified attached eddy model can be written as

$$u_z^+ = \sum_{i=1}^{N_z} a_i. \tag{2}$$

The various a's are organized hierarchically on a treelike structure as depicted in Fig. 1(b), with a_1 corresponding to the largest eddy that overlaps the entire hierarchy, a_2 taking on different values at each of the smaller eddies (two shown, but four on the plane), and so forth. Besides Ref. [9], this hierarchical additive model was recently used in Ref. [31] to provide quantitative estimates on the scalings of single-point, two-point moment-generating functions in high-Reynolds-number boundary layers. The predicted power-law behaviors in the single-point $\langle \exp(qu) \rangle$ and two-point $\langle \exp(qu + q'u(x+r)) \rangle$ moment-generating functions with respect to the wall normal distance z/δ and two-point displacement r/δ were confirmed in experimental measurements in Ref. [31]. Here we apply the formalism to elucidate logarithmic scaling laws of particular two-point moments that scale with $\ln(\delta/r)$.

One of the major results Townsend arrived at is the logarithmic scaling in the variance of streamwise velocity fluctuation:

$$\langle u_z^2 \rangle = A_1 \ln(\delta/z) + B_1, \tag{3}$$

where $A_1 \approx 1.26$ is the Townsend-Perry constant [3,32–35], B_1 is a (flow-dependent) constant, $\langle \cdot \rangle$ indicates ensemble averaging, and we have dropped henceforth the superscript $+$ (conventionally used to indicate normalization by wall units). A considerable amount of empirical evidence both from laboratory experiments and from numerical simulations has been reported recently in support of the logarithmic scaling shown in Eq. (3) [34,36].

As an example of the application of the hierarchical random additive process (HRAP) based attached eddy model, the basic scaling of Eq. (3) using Eqs. (1) and (2) can be derived simply as follows: given that a_i's are i.i.d., squaring both sides of Eq. (2) leads to

$$\langle u_z^2 \rangle = N_z \langle a^2 \rangle \sim \ln(\delta/z), \tag{4}$$

thus recovering the logarithmic scaling in $\langle u_z^2 \rangle$.

While the HRAP enables us to obtain very rapidly scaling behavior (functional forms), evaluating prefactors and additive coefficients requires more detailed modeling assumptions and more extensive calculations. For instance, in the formalism developed in Refs. [10,11], where the arrival of an attached eddy at a generic point in the flow field is assumed to be described by a Poisson process, rigorous, step-by-step derivations can be carried out to derive generalized logarithmic laws in even-order moments of single-point velocity fluctuations and even-order moments of structure functions; i.e.,

$$\langle (u_z)^{2p} \rangle^{1/p} = A_p \ln(\delta/z) + B_p,$$
$$\langle (u_z(x+r) - u_z(x))^{2p} \rangle^{1/p} = D_p \ln(r/z) + E_p, \tag{5}$$

where A_p, B_p, D_p, and E_p are coefficients. Empirical evidence for the logarithmic laws shown in Eqs. (5) was reported in Refs. [9,11,37]. Hereafter, we focus mainly on the scaling behavior and do not emphasize the typically flow-dependent coefficients B_p and E_p.

We show that predictions of the generalized logarithmic laws in Eqs. (5), as well as for the standard two-point correlation function $S_1 = \langle u_z(x) u_z(x+r) \rangle = A_1 \ln(\delta/r) + B_1'$, can be made quite easily using Eqs. (1) and (2). Moreover, the HRAP model is used in this paper to predict the existence of a new family of logarithmic laws such as

$$S_2 = \left[\frac{3}{2} \langle u_z^2(x) u_z^2(x+r) \rangle - \frac{1}{2} \langle u_z^4(x) \rangle \right]^{1/2} = A_2 \ln\left(\frac{\delta}{r}\right) + B_2', \tag{6}$$

$$S_3 = \left[\frac{5}{2} \langle u_z^3(x) u_z^3(x+r) \rangle - \frac{3}{2} \langle u_z(x) u_z^5(x+r) \rangle \right]^{1/3} = A_3 \ln\left(\frac{\delta}{r}\right) + B_3', \tag{7}$$

$$S_4 = \left[\frac{1}{10} \langle u_z^8(x) \rangle + \frac{9}{10} \langle u_z(x) u_z^7(x+r) \rangle - \frac{49}{10} \langle u_z^2(x) u_z^6(x+r) \rangle \right.$$
$$\left. - \frac{21}{10} \langle u_z^3(x) u_z^5(x+r) \rangle + \frac{70}{10} \langle u_z^4(x) u_z^4(x+r) \rangle \right]^{1/4}$$
$$= A_4 \ln\left(\frac{\delta}{r}\right) + B_4'. \tag{8}$$

Note that the two-point structure functions studied in Ref. [11] depend on $\ln(r/z)$. It will be shown that the new generalized two-point correlations depend on $\ln(\delta/r)$ instead, i.e., scaling with the boundary layer thickness rather than the local scale z. Invoking Taylor's frozen turbulence hypothesis [38], experimental hot-wire turbulence measurements from the Melbourne High Reynolds Number Boundary Layer Wind Tunnel (HRNBLWT) [39] are analyzed to test the existence of such new logarithmic laws.

The rest of the paper is organized as follows. In Sec. II, the HRAP model is used to derive various generalized logarithmic laws. Empirical evidence for the new laws is presented in Sec. III. In Sec. IV

it is shown that similar scaling can be recovered more rigorously using the formalism developed in Ref. [10]. Conclusions are given in Sec. V.

II. HIERARCHICAL RANDOM ADDITIVE PROCESS

In this section, the HRAP is used to predict the scalings of various turbulence quantities in the logarithmic region. We assume the flow is at high Reynolds number and we consider only streamwise velocity fluctuations. Unless stated otherwise, wall units are used for normalization.

In the limit of high Reynolds number, $N_z \sim \ln(\delta/z)$ tends to large values and the central limit theorem applied to the sum in Eq. (2) leads to

$$u_z = \mathcal{N}(\mu = 0, \sigma^2 = N_z\langle a^2\rangle), \tag{9}$$

where $\mathcal{N}(\mu, \sigma^2)$ is a Gaussian random variable with mean μ and variance σ^2. As argued in Ref. [9], Eq. (9) directly leads to

$$\langle u_z^{2p}\rangle = (2p-1)!!A_1^p \ln^p(\delta/z), \tag{10}$$

where A_1 is the Townsend-Perry constant mentioned before. Comparing with Eqs. (5) leads to

$$A_p^p = (2p-1)!!A_1^p. \tag{11}$$

As shown in Ref. [9], data support the logarithmic scaling of Eq. (10) but show that A_p is smaller than the Gaussian prediction of Eq. (11).

Next we consider the velocity at a point P' above P and at a distance z_1 from the wall, $z_1 > z$. Because an attached eddy that contributes to the velocity at point P' also affects point P, Eq. (2) directly leads to

$$u_z - u_{z_1} = \sum_{i=1}^{N_z} a_i - \sum_{i=1}^{N_{z_1}} a_i = \sum_{i=N_{z_1}}^{N_z} a_i,$$

$$N_z - N_{z_1} \sim \ln(\delta/z) - \ln(\delta/z_1) = \ln(z_1/z). \tag{12}$$

Following the same arguments that lead to Eq. (10), Eqs. (12) directly lead to

$$\langle (u_z(x) - u_{z_1}(x))^{2p}\rangle = (2p-1)!!A_1^p \ln^p(z_1/z). \tag{13}$$

Now we consider the velocity at P and a point P'' which is at a distance r downstream of P (as shown in Fig. 1). For small r compared to z, all eddies that affect P similarly affect P''. At a distance $r = z/\tan\theta$, where θ is the inclination angle of a typical attached eddy, P and P'' are different by at most about one eddy (one additive term) and share all eddies above z. As a result, $u_z(x)$ and $u_z(x + z/\tan\theta)$, differing by one random additive (the random additive that is associated with eddies of size z), are approximately equal because $N_z = \ln(\delta/z)$ is assumed to be large (see similar argument in Refs. [40,41]). As r further increases P and P'' share fewer and fewer common eddies.

Now let us consider the general case for arbitrary, large r in the context of two-point moments of the form $\langle u_z^n(x)u_z^{2p-n}(x+r)\rangle$. We decompose the velocity fluctuation at a point into contributions from eddies of size smaller than r (height smaller than $r\tan\theta$) and greater than r (height larger than $r\tan\theta$). Let

$$z_r = r\tan\theta \tag{14}$$

and define $u_{z\backslash z_r}(x) = u_z - u_{z_r}$, which within the additive model can be regarded as the contribution to the velocity fluctuation only from those eddies whose size is smaller than r. Then we have

$$\langle u_z^n(x)u_z^{2p-n}(x+r)\rangle = \langle [u_{z\backslash z_r}(x) + u_{z_r}(x)]^n [u_{z\backslash z_r}(x+r) + u_{z_r}(x+r)]^{2p-n}\rangle. \tag{15}$$

In the HRAP model, $u_{z \backslash z_r}(x)$ and $u_{z \backslash z_r}(x + r)$ can be considered statistically independent because eddies of size smaller than z_r cannot affect two points that are separated by a distance r. Moreover, $u_{z \backslash z_r}(x)$ and $u_{z_r}(x)$ are statistically independent [so are $u_{z \backslash z_r}(x + r)$ and $u_{z_r}(x + r)$] because eddies of different sizes are not correlated in the current version of the model since all a's are assumed independent. Combining these observations and the approximation $u_{z_r}(x) \approx u_{z_r}(x + r)$, the moments $\langle u_z^n(x) u_z^{2p-n}(x + r) \rangle$ can be evaluated.

When evaluating the products and separating them accordingly at various orders, there seems to be no compact expression for $\langle u_z^n(x) u_z^{2p-n}(x + r) \rangle$. However, since it is unlikely that there would be much interest in much higher order statistics than the eighth order moments, we can explicitly evaluate each combination of p and n for $p < 5$. As an initial example, we evaluate the standard two-point correlation function $\langle u_z(x) u_z(x + r) \rangle$ as follows:

$$
\begin{aligned}
\langle u_z(x) u_z(x + r) \rangle &= \left\langle \left(u_{z \backslash z_r}(x) + u_{z_r}(x) \right) \left(u_{z \backslash z_r}(x + r) + u_{z_r}(x + r) \right) \right\rangle \\
&= \langle u_{z \backslash z_r}(x) \rangle \langle u_{z \backslash z_r}(x + r) \rangle + 2 \langle u_{z \backslash z_r}(x) \rangle \langle u_{z_r}(x) \rangle + \langle u_{z_r}(x) u_{z_r}(x) \rangle. \quad (16)
\end{aligned}
$$

Since the the velocity fluctuation u has zero mean, we obtain

$$
\langle u_z(x) u_z(x + r) \rangle = \langle u_{z_r}(x) u_{z_r}(x) \rangle = A_1 \ln(\delta/z_r) = A_1 \ln(\delta/r) + B_1', \quad (17)
$$

where the last equality holds up to an additive coefficient B_1' that can depend on, for instance, $\tan\theta$.

Defining

$$
L_{p,n} = \ln^{p-n}(\delta/z_r) \ln^n(z_r/z), \quad (18)
$$

and following the same procedure used to obtain Eq. (17), and using Eqs. (10) and (13), we have

$$
\begin{aligned}
\langle u_z^0(x) u_z^4(x + r) \rangle &= A_2^2 L_{2,2} + 6A_1^2 L_{2,1} + A_2^2 L_{2,0}, \\
\langle u_z^1(x) u_z^3(x + r) \rangle &= 0 + A_1^2 L_{2,1} + A_2^2 L_{2,0}, \\
\langle u_z^2(x) u_z^2(x + r) \rangle &= A_1^2 L_{2,2} + A_1^2 L_{2,1} + A_2^2 L_{2,0},
\end{aligned} \quad (19)
$$

$$
\begin{aligned}
\langle u_z^0(x) u_z^6(x + r) \rangle &= A_3^3 L_{3,3} + 15A_2^2 A_1 L_{3,2} + 15A_1 A_2^2 L_{3,1} + A_3^3 L_{3,0}, \\
\langle u_z^1(x) u_z^5(x + r) \rangle &= 0 + 5A_2^2 A_1 L_{3,2} + 10A_1 A_2^2 L_{3,1} + A_3^3 L_{3,0}, \\
\langle u_z^2(x) u_z^4(x + r) \rangle &= A_2^2 A_1 L_{3,3} + \left(6A_1^3 + A_2^2 A_1\right) L_{3,2} + 7A_1 A_2^2 L_{3,1} + A_3^3 L_{3,0}, \\
\langle u_z^3(x) u_z^3(x + r) \rangle &= 0 + 9A_1^3 L_{3,2} + 6A_1 A_2^2 L_{3,1} + A_3^3 L_{3,0},
\end{aligned} \quad (20)
$$

$$
\begin{aligned}
\langle u_z^0(x) u_z^8(x + r) \rangle &= A_4^4 L_{4,4} + 28A_3^3 A_1 L_{4,3} + 70A_2^4 L_{4,2} + 28A_1 A_3^3 L_{4,1} + A_4^4 L_{4,0}, \\
\langle u_z^1(x) u_z^7(x + r) \rangle &= 0 + 7A_3^3 A_1 L_{4,3} + 35A_2^4 L_{4,2} + 21A_1 A_3^3 L_{4,3} + A_4^4 L_{4,0}, \\
\langle u_z^2(x) u_z^6(x + r) \rangle &= A_3^3 A_1 L_{4,4} + \left(15A_1^2 A_2^2 + A_3^3 A_1\right) L_{4,3} + \left(15A_1^2 A_2^2 + 15A_2^4\right) L_{4,2} \\
&\quad + 16A_1 A_3^3 L_{4,1} + A_4^4 L_{4,0}, \\
\langle u_z^3(x) u_z^5(x + r) \rangle &= 0 + 15A_1^2 A_2^2 L_{4,3} + \left(30A_1^2 A_2^2 + 5A_2^4\right) L_{4,2} + 13A_1 A_3^3 L_{4,1} + A_4^4 L_{4,0}, \\
\langle u_z^4(x) u_z^4(x + r) \rangle &= A_2^4 L_{4,4} + 12A_1^2 A_2^2 L_{4,3} + \left(36A_1^2 A_2^2 + 2A_2^4\right) L_{4,2} + 12A_1 A_3^3 L_{4,1} + A_4^4 L_{4,0},
\end{aligned} \quad (21)
$$

The A_p's in Eqs. (19)–(21) can be replaced with $[(2p - 1)!!]^{1/p} A_1$ to further simplify the expressions (not shown here).

We make three observations. First, except for $n = 0$ and $n = p$, all $L_{p,n}$'s are mixed logarithmic scalings involving different powers of $\ln(\delta/z_r)$ and $\ln(z_r/z)$. At high Reynolds number, as $r/z \to \infty$ (and $z_r/z \to \infty$), for $\delta/z_r \sim O(1)$, $L_{p,p}$ becomes the dominant term; as $r/z \sim O(1)$, $\delta/r \to \infty$,

$L_{p,0}$ becomes the dominant term. As a result, in those limits logarithmic scaling can be observed in quantities such as $\langle u_z^n(x)u_z^{2p-n}(x+r)\rangle^{1/p}$. This aspect is, however, not further explored here. Second, for a fixed p, the coefficient in front of the term $L_{p,0}$ is A_p^p and is not dependent on n.

Third, the traditionally defined two-point structure functions $\langle [u_z(x) - u_z(x+r)]^{2p}\rangle$ [in Eqs. (5)], being combinations of $\langle u_z^n(x)u_z^{2p-n}(x+r)\rangle$, i.e.,

$$\langle (u_z(x) - u_z(x+r))^{2p}\rangle^{1/p} = \left[\sum_{n=0}^{2p} C_{2p}^n \langle u_z^n(x)u_z^{2p-n}(x+r)\rangle\right]^{1/p}, \tag{22}$$

where $C_{2p}^n = (2p)!/[n!(2p-n)!]$, can be shown to depend only on the term $L_{p,p}$. In order to verify this, we compute, for example, $\langle (u_z(x) - u_z(x+r))^6\rangle$:

$$\langle (u_z(x) - u_z(x+r))^6\rangle = 2\langle u_z^0(x)u_z^6(x+r)\rangle - 12\langle u_z^1(x)u_z^5(x+r)\rangle$$
$$+ 30\langle u_z^2(x)u_z^4(x+r)\rangle - 20\langle u_z^3(x)u_z^3(x+r)\rangle. \tag{23}$$

Substituting Eqs. (20) into Eq. (23) indeed leads to

$$\langle (u_z(x) - u_z(x+r))^6\rangle = (2A_3^3 + 30A_2^2 A_1)L_{3,3} = (2A_3^3 + 30A_2^2 A_1)\ln(z_r/z) \sim \ln(r/z), \tag{24}$$

i.e., one obtains an exact cancellation of all $L_{p,n}$'s for $n < p$. The same cancellations are found for structure functions of second order, fourth order, eighth order, etc. (not shown here). Hence we recover the logarithmic scaling in structure functions (such scaling has been explored based on experimental data in Ref. [11]).

Structure functions thus pick up the logarithmic scaling $\ln(r/z)$, i.e., the term $L_{p,p}$. The other term that does not contain mixed logarithmic scalings is $L_{p,0}$. We attempt to find combinations of $\langle u_z^n(x)u_z^{2p-n}(x+r)\rangle$ such that all $L_{p,n}$, $n > 0$, cancel except for $L_{p,0}$. Formally, for a fixed p, we attempt to find c_n's such that

$$\sum_{n=0}^{p} c_n \langle u_z^n(x)u_z^{2p-n}(x+r)\rangle = A_p^p L_{p,0}. \tag{25}$$

The new logarithmic laws in Eqs. (6)–(8) are obtained by solving Eq. (25) for the c_n's. Here, as an example, we verify S_3:

$$\left[\tfrac{5}{2}\langle u_z^3(x)u_z^3(x+r)\rangle - \tfrac{3}{2}\langle u_z(x)u_z^5(x+r)\rangle\right]^{1/3} = \left[A_3^3 L_{3,0} + \left(\tfrac{45}{2}A_1^3 - \tfrac{15}{2}A_2^2 A_1\right)L_{3,2}\right]^{1/3}. \tag{26}$$

Using Eq. (10) (i.e., $A_2^2 = 3A_1^2$), Eq. (26) leads to

$$\left[\tfrac{5}{2}\langle u_z^3(x)u_z^3(x+r)\rangle - \tfrac{3}{2}\langle u_z(x)u_z^5(x+r)\rangle\right]^{1/3} = A_3 L_{3,0}^{1/3} = A_3 \ln(\delta/r) + B_3'. \tag{27}$$

S_2 and S_4 can be verified in the same manner and again the relation $A_p^p = (2p-1)!!A_1^p$ needs to be used to ensure exact cancellation of $L_{p,n}$, $n > 0$. Notice that the term that remains when evaluating S_i, $i = 1,2,3,4$, comes from $\langle (u_z - u_{z_r})^{2p}\rangle = A_p^p \ln^p(z/r)$, and the predicted slopes in those logarithmic laws are directly expressed in terms of A_p ($p = 1,2,3,4$) and not as $(2p-1)!!A_p^p$. As a result, for a comparison of the slopes predicted in those logarithmic scalings (in Sec. III), we use the measured A_p's instead of the Gaussian predictions $A_p = [(2p-1)!!]^{1/p}A_1$.

Up to here we have derived, using the HRAP model, the previously known logarithmic laws [Eqs. (5)] and new ones [Eqs. (6)–(8)]. Supporting empirical evidence for the new logarithmic laws in Eqs. (6)–(8) is presented below in Sec. III.

III. EXPERIMENTAL DATA ANALYSIS

In this section, the logarithmic scalings in Eqs. (6)–(8) are examined using the Melbourne wind tunnel measurements. The Reynolds number based on boundary layer height and friction velocity is
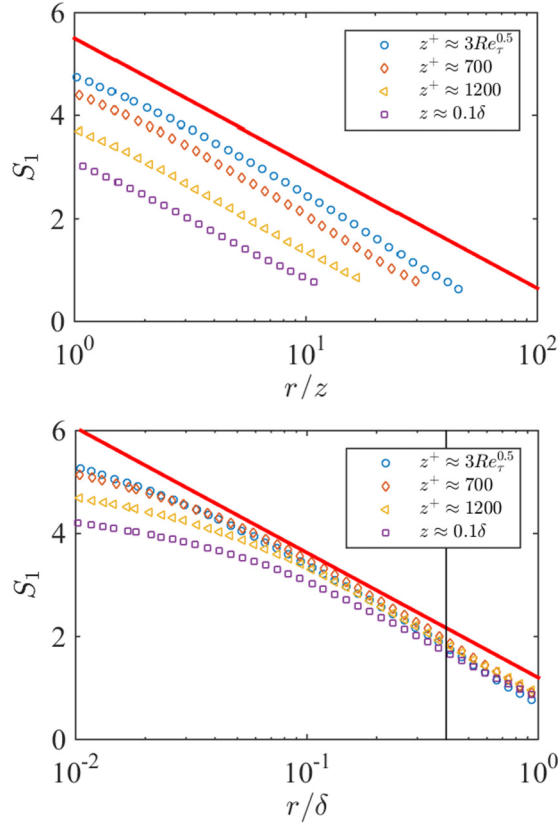
FIG. 2. S_1 against r/z (top), r^+ (bottom) at $z^+ \approx 3\mathrm{Re}_\tau^{0.5}$, 700, 1200, and $z = 0.10\delta$. The solid line indicates the fitted slope. $r/\delta = 0.4$ is indicated with a vertical line.

$\mathrm{Re}_\tau = 19\,030$ (see Ref. [39] for more details of the data set). The analysis focuses on the scaling in r in the inertial region. The Taylor frozen turbulence hypothesis is invoked to convert the temporal data from hot-wire measurements to spatial data [38,42].

Statistical two-point moments as defined in Eqs. (6)–(8) are plotted against r^+ and r/z at various heights, namely, at $z^+ \approx 3\mathrm{Re}_\tau^{0.5}$, 700, 1200 and $z = 0.10\delta$ in Figs. 2–5. Solid lines show fitted slopes, 1.1, 1.5, 2.0, and 1.8, respectively, for S_1, S_2, S_3, and S_4. Compared with the measured A_p values from Ref. [9], i.e., $A_1 \approx 1.2$, $A_2 \approx 1.8$, $A_3 \approx 2.4$, and $A_4 \approx 3.00$, given the uncertainty in the measurements both here and in Ref. [9], the agreement is reasonably good, except for S_4. The fit is conducted within the logarithmic region and averaged over the four wall normal locations. The start of the logarithmic region is at around $z^+ = 3\mathrm{Re}_\tau^{0.5}$. No logarithmic scaling as indicated in Eqs. (6)–(8) is expected at $z^+ < 3\mathrm{Re}_\tau^{0.5}$, nor above $z^+ = 0.15\delta$, which is the end of the logarithmic region [34]. At a specific wall normal location in the logarithmic region, i.e., following Ref. [34], in $3\mathrm{Re}_\tau^{0.5} < z^+$, $z < 0.15\delta$, one expects to observe the logarithmic scalings in Eqs. (6)–(8) in a range of two-point displacement r that corresponds to flow structures whose elongation is associated with wall distances z belonging to the logarithmic region. To obtain a crude estimate of this range, we note that an attached eddy of size h in the vertical direction can affect a distance of $h/\tan\theta$ in the flow direction, where θ is the inclination angle of an attached eddy. At a height z, an attached eddy of height $h < z$ is not relevant and, therefore, the relevant r range is expected to begin at $r > z/\tan\theta$. At large displacements, by this argument, the end of the logarithmic scaling occurs at $r = 0.15\delta/\tan\theta$. The typically observed inclination angle of an attached eddy is $\theta \approx 11°–16°$ [43–46]. This leads to an expected range of
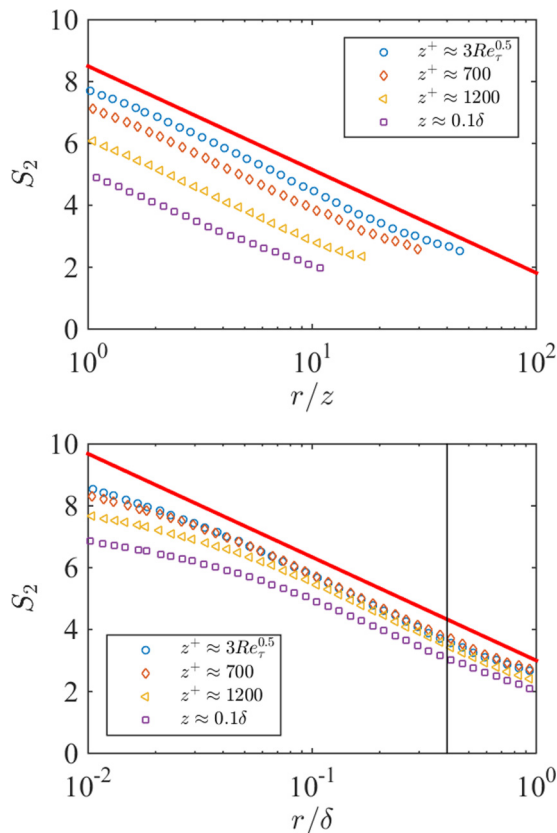
FIG. 3. Same as Fig. 2, but for S_p ($p = 2$).

logarithmic scaling $z/\tan\theta < r < 0.15\delta/\tan\theta$, which is approximately $4z < r < 0.6\delta$. Practically, the relevant range of r, within which logarithmic scaling can be observed, can differ from this estimate and can vary depending on the specific statistical quantity under consideration. However, this estimate is instructive as it correctly points out that the start of the logarithmic scaling in r depends on z and the end on the boundary layer height. With this understanding, we examine Figs. 2–5 in detail. First, by plotting against r/z, the starting point of the logarithmic region can be determined. At $z^+ = 3\mathrm{Re}_\tau^{0.5}$, slight deviations from logarithmic scaling can be observed for S_1 and S_2 from $r/z \approx 2$ to the left. For S_3 and S_4 at $z^+ = 3\mathrm{Re}_\tau^{0.5}$ and for all S_i, $i = 1, 2, 3, 4$, at $z^+ = 700$, 1200, 1900 ($z = 0.1\delta$), logarithmic scalings start at $r = z$. Hence, $r = z$ is probably a safe estimate for the start point of the logarithmic scalings. The end of the logarithmic scaling is better determined by plotting the two-point moments against r/δ. For $S_1 = \langle u_z(x)u_z(x + r)\rangle$, the logarithmic scaling is found to extend at least up to $r = \delta$ (and even beyond). For S_2 and S_3, flattening of the scaling (decrease in the slope) is found at around $r^+ = 8000$ ($r = 0.4\delta$). The end point of the logarithmic scalings is therefore around $r = 0.4\delta$ for S_2 and S_3. A lack of data convergence for S_4 makes determining the end point of logarithmic scaling of S_4 difficult, but the data are not inconsistent with the estimate $r = 0.4\delta$. In sum, empirically, the logarithmic scaling can be observed in $z < r < 0.4\delta$. To ensure the existence of such a region and at the same time ensure that the measurements remain in the logarithmic region, the analysis must be restricted to heights such that $3\mathrm{Re}_\tau^{0.5} < z^+$, $z < 0.15\delta$.

The undulations seen in Fig. 5 at large r are due to a lack of full statistical convergence. Limited by the size of the data, we therefore do not consider statistics of higher order. As can be seen, the statistics in Eqs. (6)–(8) follow the predicted logarithmic scaling rather closely, at least within the expected
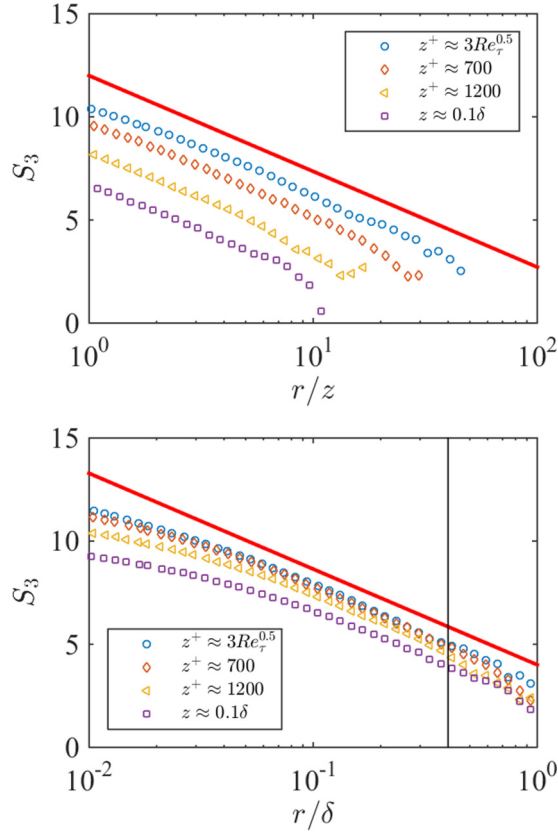
FIG. 4. Same as Fig. 2, but for S_3.

range of r. In contrast to $\langle(u_z^+(x+r) - u_z^+(x))^{2p}\rangle^{1/p}$, plotting against r/z does not collapse the data; instead, by plotting against r^+ (or against r/δ) a better collapse is obtained (although evidently not a full collapse). In Eqs. (19)–(21), neglecting additive constants and equating $\langle u^{2p}\rangle^{1/p}$ to $\ln(\delta/z)$ is unlikely to cause this lack of collapse because the additive constants can be absorbed as a single multiplying factor of the outer length scale δ. The lack of full collapse is possibly due to a lack of exact cancellation of $L_{p,n}$, $n > 0$. Exact cancellation of $L_{p,n}$, $n > 0$, in the framework of the HRAP depends, for the logarithmic scalings in Eqs. (6)–(8), critically on $A_p = [(2p-1)!!]^{1/p}A_1$ [see Eqs. (26) and (27)], i.e., on wall eddies being noninteracting and, equivalently, on a_i in Eq. (2) being i.i.d. In reality, eddies clustering can lead to significant correlations among the attached eddies [23]. A_p can then differ from $[(2p-1)!!]^{1/p}A_1$, leading to the lack of complete collapse of the logarithmic scalings at different wall normal heights. Observed slopes in the logarithmic laws agree reasonably well with the model predictions (considering the uncertainty in the measurements), which indirectly confirms Eq. (13) [notice $L_{p,0} = \ln(\delta/r)$ is based on Eq. (13)], although some deviations are observed, especially for high order statistics.

Next we verify the statistical convergence of the moments shown in Figs. 2–5. To achieve statistical convergence of higher order statistics (sixth and eighth order statistics) one requires larger amounts of data and it is more challenging as compared to the convergence in lower order statistics (second and fourth order). Here we examine the premultiplied joint probability density function (PDF) of $u_z(x)$ and $u_z(x+r)$. The two plots are relevant for the evaluation of $\langle u_z(x)u_z^7(x+r)\rangle$ and $\langle u_z^4(x)u_z^4(x+r)\rangle$. A representative wall distance $z^+ = 1400$ and a relatively large streamwise
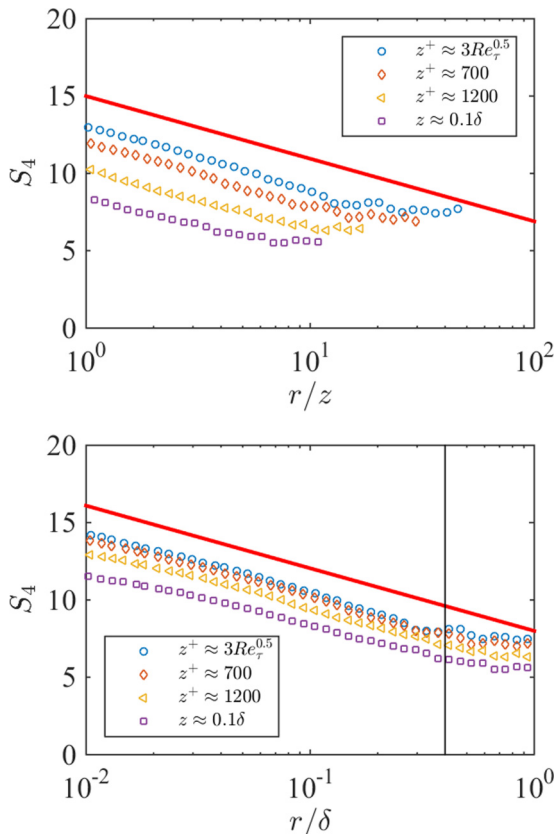
FIG. 5. Same as Fig. 2, but for S_4.

separation $r = 0.3\delta$ (which is a more challenging case compared to small streamwise separations) is considered. Figure 6 shows the premultiplied joint PDF. As can be seen from Fig. 6, the two-point moments under consideration, which is essentially the area (volume) under the surface, can be reasonably captured by the amount of data available as the probability density goes to zero at the high values.

IV. A MORE RIGOROUS DERIVATION OF THE NEW LOGARITHMIC LAWS

In this section, we derive the logarithmic scalings in Eqs. (6)–(8) in a more rigorous manner using the formalism developed in Ref. [10]. The goal here is to show that the new logarithmic laws are not dependent on the exact details of the attached eddy formulation but depend on the essential structure of the model. We only need to show that the attached eddy formulation used in Ref. [10] gives the same prediction for the two-point velocity fluctuation correlations raised to arbitrary powers [i.e., $\langle u_z^n(x) u_z^{2p-n}(x + r) \rangle$].

Following Ref. [10], the streamwise velocity fluctuation at a point is expressed as

$$u(\mathbf{x}) = \sum_k Q_x \left(\frac{\mathbf{x} - \mathbf{x}_{e_k}}{h_k} \right), \tag{28}$$

where $Q_x((\mathbf{x} - \mathbf{x}_{e_k})/h_k)$ is the streamwise velocity fluctuation at a point $\mathbf{x}$ induced by a typical attached eddy of size h_k located at $\mathbf{x}_{e_k}$ and the sum is over all eddies in the domain. The inclination
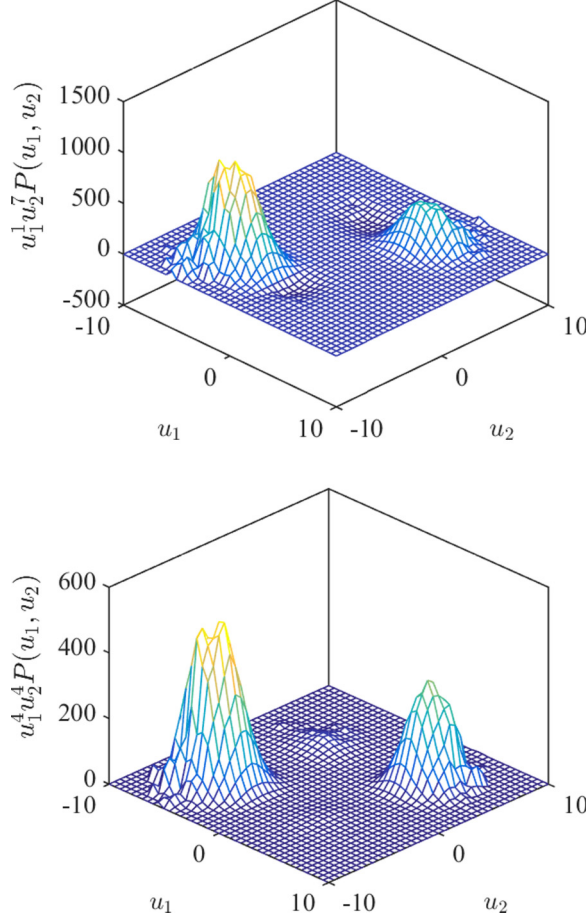
FIG. 6. Premultiplied PDF for $u_z(x)u_z^7(x+r)$ and $u_z^4(x)u_z^4(x+r)$ at a vertical height $z^+ = 1400$ and a streamwise separation $r = 0.3\delta$. $u_1 = u_z(x)$ and $u_2 = u_z(x+r)$. The two-point PDF $P(u_1, u_2)$ corresponds to the two points $u_1 = u_z(x)$ and $u_2 = u_z(x+r)$.

angle of a typical eddy is θ and it follows that the extent of a typical eddy at height z_r covers a streamwise distance $r = z_r / \tan\theta$.

Decomposing the right-hand side of Eq. (28) into contributions from eddies of size smaller than z_r and eddies of size larger than z_r leads to

$$u(\mathbf{x}) = \sum_{h_k < z_r} Q_x\left(\frac{\mathbf{x} - \mathbf{x}_{e_k}}{h_k}\right) + \sum_{h_k > z_r} Q_x\left(\frac{\mathbf{x} - \mathbf{x}_{e_k}}{h_k}\right). \tag{29}$$

Performing the same decomposition on the velocity fluctuation at $\mathbf{x} + \mathbf{i}r$, where $\mathbf{i}$ is the unit vector in the streamwise direction, leads to

$$u(\mathbf{x} + \mathbf{i}r) = \sum_{h_k < z_r} Q_x\left(\frac{\mathbf{x} + \mathbf{i}r - \mathbf{x}_{e_k}}{h_k}\right) + \sum_{h_k > z_r} Q_x\left(\frac{\mathbf{x} + \mathbf{i}r - \mathbf{x}_{e_k}}{h_k}\right). \tag{30}$$

Following the same arguments that lead to $u_z(x) \approx u_z(x+r)$, we have

$$\sum_{h_k > z_r} Q_x\left(\frac{\mathbf{x} + \mathbf{i}r - \mathbf{x}_{e_k}}{h_k}\right) \approx \sum_{h_k > z_r} Q_x\left(\frac{\mathbf{x} - \mathbf{x}_{e_k}}{h_k}\right). \tag{31}$$

Equations (29)–(31) lead to

$$\langle u^n(\mathbf{x})u^{2p-n}(\mathbf{x}+\mathbf{i}r)\rangle = \left\langle \left[\sum_{h_k<z_r} Q_x\left(\frac{\mathbf{x}-\mathbf{x}_{e_k}}{h_k}\right) + \sum_{h_k>z_r} Q_x\left(\frac{\mathbf{x}-\mathbf{x}_{e_k}}{h_k}\right) \right]^n \right.$$

$$\left. \times \left[\sum_{h_k<z_r} Q_x\left(\frac{\mathbf{x}+\mathbf{i}r-\mathbf{x}_{e_k}}{h_k}\right) + \sum_{h_k>z_r} Q_x\left(\frac{\mathbf{x}-\mathbf{x}_{e_k}}{h_k}\right) \right]^{2p-n} \right\rangle. \quad (32)$$

Expanding the right-hand side of Eq. (32) gives rise to terms like

$$\left\langle \left[\sum_{h_k<z_r} Q_x\left(\frac{\mathbf{x}-\mathbf{x}_{e_k}}{h_k}\right) \right]^{p_1} \right\rangle \left\langle \left[\sum_{h_k<z_r} Q_x\left(\frac{\mathbf{x}+\mathbf{i}r-\mathbf{x}_{e_k}}{h_k}\right) \right]^{p_2} \right\rangle \left\langle \left[\sum_{h_k>z_r} Q_x\left(\frac{\mathbf{x}-\mathbf{x}_{e_k}}{h_k}\right) \right]^{p_3} \right\rangle.$$

We now recall that Ref. [10] [their Eqs. (18) and (23)] proves that

$$\left\langle \left[\sum_{k,h_1<h_k<h_2} Q_x\left(\frac{\mathbf{x}-\mathbf{x}_{e_k}}{h_k}\right) \right]^{2p'} \right\rangle = A_{p'}^{p'} \ln^{p'}\left(\frac{h_2}{\max(z,h_1)}\right) \quad (33)$$

by considering the size of the smallest eddy being h_1 and the size of the largest eddy being h_2. Then, by using Eqs. (32) and (33), we can recover the predictions for $\langle u_z^n(x)u_z^{2p-n}(x+r)\rangle$ made using the HRAP formalism [i.e., Eqs. (19)–(21)] and with Eqs. (19)–(21) the new logarithmic laws in Eqs. (6)–(8) can be verified. This completes the proof of the new logarithmic laws [in Eqs. (6)–(8)] using the formalism developed in Ref. [10].

V. CONCLUSIONS

New logarithmic laws [Eqs. (6)–(8)] for wall-bounded flows can be predicted if one follows the HRAP formalism to its logical conclusion. The HRAP model enables us to easily make predictions about scaling behaviors in turbulence statistics (including conventional moments and the moment-generating function [31]) in the logarithmic region at high Reynolds numbers. Empirical evidence supporting the newly predicted logarithmic laws are presented by analyzing the $\mathrm{Re}_\tau = 19\,030$ data set [39]. We also arrive at the logarithmic laws in Eqs. (6)–(8) using the formulation developed in Ref. [10] in a more rigorous manner. Those newly found logarithmic laws provide additional support to the basic hierarchical structure of wall-bounded eddies hypothesized by Townsend and can be used for model and code validation as well as for discriminating among different simplified models of wall eddies.

We recognize also that not all flow statistics can be correctly predicted within the present HRAP framework, even when restricting attention in the logarithmic inertial region. For instance, both the attached model developed in Ref. [10] and the HRAP used in this work predict a collapse of the new logarithmic scalings using $\ln(\delta/r)$ at different wall normal distances at high Reynolds number. However, the experimental data do not show a full collapse using $\ln(\delta/r)$ [although the collapse is appreciably better using $\ln(\delta/r)$ compared to using $\ln(z/r)$; the latter was previously used to collapse the structure functions $\langle(u(z,x) - u(z,x+\mathbf{i}r))^{2p}\rangle^{1/p}$ [11]]. It is possible that the discrepancies could be due to coherent motions in the logarithmic layer. That is to say, a lack of correlations among the random additive terms may be responsible for the differences between HRAP model predictions and experimental observations. Besides the lack in accounting for correlations among eddies of different sizes in the hierarchy, HRAP as presented does not include magnitude modulation of small-scale velocity fluctuations near the wall by larger-scale eddies further above the wall, a mechanism that is found to be prevalent in high-Reynolds-number wall-bounded flows [47,48]. However, the "outer peak" which is responsible for the modulation of the near-wall motions corresponds, in the current version of the HRAP, to the last step in the hierarchy. One can view the outcome of the HRAP as the outer scale input to the wall modulation approach [48].

Hence more refined eddy models and extensions of the HRAP approach including more detailed physics beyond the simple additive superposition of independent eddy-induced velocity fluctuations can be considered in the future. We believe that the more advanced statistical diagnostic tools provided here by the new generalized two-point moments (S_1, S_2, S_3, S_4, etc.) can be used to test those possible extensions.

As logarithmic scalings with respect to the wall normal distance can be found in the even order moments of the spanwise velocity components, i.e., $\langle v^2 \rangle \sim \ln(\delta/z)$, it could be expected that the spanwise velocity fluctuation should follow a similar additive process, and the derived scalings here may be observed also for the spanwise velocity. Moreover, because the attached eddies have a finite span in the transverse direction, those two-point logarithmic scalings are expected to hold if the two-point displacement is instead in the transverse direction. For the data sets used in this work, those ideas cannot be studied. Further investigations with additional data should examine the detailed structure of the spanwise velocity and two-point logarithmic scalings that involves a spanwise displacements. Based also on previous work [11], while we do expect the logarithmic dependencies to exist for v, we do not expect to see them for w (the wall normal component).

[1] T. von Kármán, Mechanische aehnlichkeit und turbulenz, in *Proceedings of the Third International Congress of Applied Mechanics* (P. A. Norstedt & Soner, Stockholm, 1930), Vol. 1, p. 79.

[2] L. Prandtl, Bericht ueber Untersuchungen zur ausgebildeten Turbulenz, Z. Angew. Math. Mech. **5**, 136 (1925).

[3] A. J. Smits, B. J. McKeon, and I. Marusic, High-Reynolds number wall turbulence, Annu. Rev. Fluid Mech. **43**, 353 (2011).

[4] A. A. Townsend, *The Structure of Turbulent Shear Flow* (Cambridge University Press, Cambridge, UK, 1976).

[5] A. E. Perry and M. S. Chong, On the mechanism of wall turbulence, J. Fluid Mech. **119**, 173 (1982).

[6] A. E. Perry, S. Henbest, and M. S. Chong, A theoretical and experimental study of wall turbulence, J. Fluid Mech. **165**, 163 (1986).

[7] I. Marusic and N. Hutchins, Study of the log-layer structure in wall turbulence over a very large range of Reynolds number, Flow Turbul. Combust. **81**, 115 (2008).

[8] J. Jimenez and S. Hoyas, Turbulent fluctuations above the buffer layer of wall-bounded flows, J. Fluid Mech. **611**, 215 (2008).

[9] C. Meneveau and I. Marusic, Generalized logarithmic law for high-order moments in turbulent boundary layers, J. Fluid Mech. **719**, R1 (2013).

[10] J. D. Woodcock and I. Marusic, The statistical behaviour of attached eddies, Phys. Fluids **27**, 015104 (2015).

[11] C. M. de Silva, I. Marusic, J. D. Woodcock, and C. Meneveau, Scaling of second- and higher-order structure functions in turbulent boundary layers, J. Fluid Mech. **769**, 654 (2015).

[12] S. K. Robinson, Coherent motions in the turbulent boundary layer, Annu. Rev. Fluid Mech. **23**, 601 (1991).

[13] J. Jiménez, Cascades in wall-bounded turbulence, Annu. Rev. Fluid Mech. **44**, 27 (2011).

[14] M. R. Head and P. Bandyopadhyay, New aspects of turbulent boundary-layer structure, J. Fluid Mech. **107**, 297 (1981).

[15] R. J. Adrian, C. D. Meinhart, and C. D. Tomkins, Vortex organization in the outer region of the turbulent boundary layer, J. Fluid Mech. **422**, 1 (2000).

[16] N. Hutchins, W. T. Hambleton, and I. Marusic, Inclined cross-stream stereo particle image velocimetry measurements in turbulent boundary layers, J. Fluid Mech. **541**, 21 (2005).

[17] X. Wu and P. Moin, Direct numerical simulation of turbulence in a nominally zero-pressure-gradient flat-plate boundary layer, J. Fluid Mech. **630**, 5 (2009).

[18] P. Schlatter, Q. Li, R. Örlü, F. Hussain, and D. S. Henningson, On the near-wall vortical structures at moderate Reynolds numbers, Eur. J. Mech. B Fluids **48**, 75 (2014).

[19] A. J. Grass, R. J. Stuart, and M. Mansour-Tehrani, Vortical structures and coherent motion in turbulent flow over smooth and rough boundaries, Philos. Trans. R. Soc. London A **336**, 35 (1991).

[20] K. T. Christensen and R. J. Adrian, Statistical evidence of hairpin vortex packets in wall turbulence, J. Fluid Mech. **431**, 433 (2001).

[21] C. D. Tomkins and R. J. Adrian, Spanwise structure and scale growth in turbulent boundary layers, J. Fluid Mech. **490**, 37 (2003).

[22] B. Ganapathisubramani, E. K. Longmire, and I. Marusic, Characteristics of vortex packets in turbulent boundary layers, J. Fluid Mech. **478**, 35 (2003).

[23] J. d. Álamo, J. Jimenez, P. Zandonade, and R. D. Moser, Self-similar vortex clusters in the turbulent logarithmic region, J. Fluid Mech. **561**, 329 (2006).

[24] R. J. Adrian, Hairpin vortex organization in wall turbulence, Phys. Fluids **19**, 041301 (2007).

[25] A. Lozano-Durán and J. Jiménez, Time-resolved evolution of coherent structures in turbulent channels: Characterization of eddies and cascades, J. Fluid Mech. **759**, 432 (2014).

[26] J. Jimenez, J. C. Del Alamo, and O. Flores, The large-scale dynamics of near-wall turbulence, J. Fluid Mech. **505**, 179 (2004).

[27] J. C. Del Alamo, J. Jiménez, P. Zandonade, and R. D. Moser, Scaling of the energy spectra of turbulent channels, J. Fluid Mech. **500**, 135 (2004).

[28] J. d. Álamo and J. Jimenez, Linear energy amplification in turbulent channels, J. Fluid Mech. **559**, 205 (2006).

[29] A. E. Perry and I. Marusic, A wall-wake model for the turbulence structure of boundary layers. Part 1. Extension of the attached eddy hypothesis, J. Fluid Mech. **298**, 361 (1995).

[30] I. Marusic and A. E. Perry, A wall-wake model for the turbulence structure of boundary layers. Part 2. Further experimental support, J. Fluid Mech. **298**, 389 (1995).

[31] X. I. A. Yang, I. Marusic, and C. Meneveau, Moment generating functions and scaling laws in the inertial layer of turbulent wall-bounded flows, J. Fluid Mech. **791**, R2 (2016).

[32] I. Marusic and G. J. Kunkel, Streamwise turbulence intensity formulation for flat-plate boundary layers, Phys. Fluids **15**, 2461 (2003).

[33] M. Hultmark, M. Vallikivi, S. C. C. Bailey, and A. J. Smits, Turbulent Pipe Flow at Extreme Reynolds Numbers, Phys. Rev. Lett. **108**, 094501 (2012).

[34] I. Marusic, J. P. Monty, M. Hultmark, and A. J. Smits, On the logarithmic region in wall turbulence, J. Fluid Mech. **716**, R3 (2013).

[35] I. Marusic, The logarithmic region of wall turbulence: Universality, structure and interactions, in *Proceedings of the Eighteenth Australasian Fluid Mechanics Conference, Launceston, Australia, 2012*, edited by P. A. Brandner and B. W. Pearce (Australasian Fluid Mechanics Society, 2012).

[36] M. Hultmark, A theory for the streamwise turbulent fluctuations in high Reynolds number pipe flow, J. Fluid Mech. **707**, 575 (2012).

[37] R. J. A. M. Stevens, M. Wilczek, and C. Meneveau, Large-eddy simulation study of the logarithmic law for second- and higher-order moments in turbulent wall-bounded flow, J. Fluid Mech. **757**, 888 (2014).

[38] G. I. Taylor, The spectrum of turbulence, Proc. R. Soc. London A **164**, 476 (1938).

[39] N. Hutchins, T. B. Nickels, I. Marusic, and M. S. Chong, Hot-wire spatial resolution issues in wall-bounded turbulence, J. Fluid Mech. **635**, 103 (2009).

[40] C. Meneveau and A. B. Chhabra, Two-point statistics of multifractal measures, Physica A **164**, 564 (1990).

[41] J. O'Neil and C. Meneveau, Spatial correlations in turbulence: Predictions from the multifractal formalism and comparison with experiments, Phys. Fluids **5**, 158 (1993).

[42] U. Piomelli, J.-L. Balint, and J. M. Wallace, On the validity of Taylor's hypothesis for wall-bounded flows, Phys. Fluids A **1**, 609 (1989).

[43] G. L. Brown and A. S. W. Thomas, Large structure in a turbulent boundary layer, Phys. Fluids **20**, S243 (1977).

[44] S. K. Robinson, Instantaneous velocity profile measurements in a turbulent boundary layer, Chem. Eng. Commun. **43**, 347 (1986).

[45] R. S. Boppe, W. L. Neu, and H. Shuai, Large-scale motions in the marine atmospheric surface layer, Boundary Layer Meteorol. **92**, 165 (1999).

[46] I. Marusic and W. D. C. Heuer, Reynolds Number Invariance of the Structure Inclination Angle in Wall Turbulence, Phys. Rev. Lett. **99**, 114504 (2007).

[47] I. Marusic, R. Mathis, and N. Hutchins, Predictive model for wall-bounded turbulent flow, Science **329**, 193 (2010).

[48] R. Mathis, N. Hutchins, and I. Marusic, A predictive inner-outer model for streamwise turbulence statistics in wall-bounded flows, J. Fluid Mech. **681**, 537 (2011).